Progress in Organic Coatings 168 (2022) 106883

Contents lists available at ScienceDirect

Progress in Organic Coatings

journal homepage: www.elsevier.com/locate/porgcoat

Antioxidant coatings from elastomeric vinyl acetate-vinyl laurate copolymers with reduced bacterial adhesion

Marta Fadda [a,b,*], Marco Contardi [a], Silvia Dante [c], Marta Di Carlo [d], Giacoma Galizzi [d], Athanassia Athanassiou [a], Ilker S. Bayer [a,**]

[a] Smart Materials, Istituto Italiano di Tecnologia (IIT), Via Morego 30, 16163 Genoa, Italy
[b] Dipartimento di Informatica, Bioingegneria, Robotica e Ingegneria dei Sistemi (DIBRIS), University of Genoa, Via all'Opera Pia 13, 16145 Genoa, Italy
[c] Materials Characterization Facility, Istituto Italiano di Tecnologia (IIT), Via Morego 30, 16163 Genoa, Italy
[d] Istituto per la Ricerca e l'Innovazione Biomedica (IRIB), Consiglio Nazionale delle Ricerche (CNR), Via Ugo La Malfa 153, 90146 Palermo, Italy

ARTICLE INFO

Keywords:
Vinyl acetate
Curcumin
Antioxidant
Low bacterial-adhesion
Food packaging

ABSTRACT

A vinyl laurate-based elastomeric copolymer, developed as chewing gum base, was used to produce functional coatings with the antioxidant curcumin. Both the polymer and curcumin were dissolved in MIBK, methyl isobutyl ketone. Coatings were applied on glass but also on natural alginate and gelatin film surfaces by dip-coating. Microscopy analysis indicated that coatings had very homogenous surface and curcumin was effectively encapsulated within the polymeric matrix. In addition, curcumin-laden coatings (10 wt%) remained transparent with excellent UV filtering properties. The flexibility of alginate and gelatin films was maintained after coating, whereas their hydrophobicity and water vapor barrier properties improved. Furthermore, coating biocompatibility and low bacterial adhesion properties were confirmed by cell proliferation and bacterial surface contamination experiments, respectively. The radical scavenging activity of the coating was assessed with both DPPH and ABTS assay, revealing effective antioxidant properties. In addition, in weak acetic acid solutions, curcumin could be released in a sustained manner from the coatings. This coating can be used as a suitable option for improving the antioxidant and bacterial resistance properties of natural polymer films including food packaging or other relevant applications.

1. Introduction

Vinyl acetate (VAc) based polymers are widely used as adhesives for paper and wood bonding [1]. A typical example is polyvinyl acetate (PVAc), which is a non-toxic, inexpensive, biodegradable polymer [2]. It is also prone to bio-deterioration by fungi [3]. The applications of PVAc are various, such as adhesives, coatings, emulsifiers, paints, and precursor in the synthesis of polyvinyl alcohol (PVA) [4]. VAc is often copolymerized with other monomers to overcome some drawbacks of the PVAc, such as low thermal stability or weak resistance to humidity and partial hydrolysis [5]. Vinyl acetate is usually copolymerized with vinyl chloride [6,7], or acrylate [8] to produce latexes with a wide range of properties [9]. For instance, vinyl acetate-butyl acrylate emulsion copolymer is extensively used for architectural applications [9]. The ethylene-vinyl acetate copolymer (EVA) is well-known and used for a wide range of applications such as paints, encapsulation of photovoltaic modules [10], and for drug delivery systems due to its non-toxicity and biocompatibility [11]. More recently, composites of PVAc with natural polymers have also been developed [4]. For instance, Chaabouni et al. prepared an adhesive nanocomposite to improve the mechanical properties of the PVAc with cellulose nanofibrils [12]; Samaha et al. performed graft copolymerization of the VAc monomer onto corn starch in an aqueous solution with a redox initiation system [13]; Zia-ud-Din et al. improved the thermal stability of a starch-based wood adhesive using the co-monomers VAc and butyl-acrylate to promote the graft copolymerization [14]; Don et al. made a chitosan-*graft*-poly(vinyl acetate) copolymer, increasing the toughness and the water-resistance of chitosan, for particular membrane applications [15]; Silva et al. blended PVAc with sugar cane bagasse lignin demonstrating that lignin protected PVAc from photochemical degradation [16].

The monomer vinyl laurate (VL) is a vinyl ester that is mainly used in acylation processes [17,18]. It was demonstrated to be biocompatible

* Correspondence to: M. Fadda, Smart Materials, Istituto Italiano di Tecnologia (IIT), Via Morego 30, 16163 Genoa, Italy.
** Correspondence to: I.S. Bayer, Smart Materials, Istituto Italian di Tecnologia (IIT), Via Morego 30, 16163 Genoa, Italy.
E-mail addresses: marta.fadda@iit.it (M. Fadda), ilker.bayer@iit.it (I.S. Bayer).

https://doi.org/10.1016/j.porgcoat.2022.106883
Received 17 January 2022; Received in revised form 5 April 2022; Accepted 15 April 2022
Available online 25 April 2022

and non-toxic in different in vitro and in vivo models [19–21]. Moreover, it was implemented in various copolymerization processes. For instance, Sun et al. developed a carboxyl-terminated *N*-isopropylacrylamide/VL copolymer coupled with chitosan as a vector for gene transfection [22]; Abidi et al. demonstrated that cotton grafted with VL had good water repellency properties, also after repeated treatment with plasma [23]; Benee et al. developed a microgel system based on *N*-isopropylacrylamide *co*-polymerized with VL [24]; Aldakkan et al. developed nanoparticles with a poly(vinyl laurate-*co*-vinyl acetate) core and poly(ethylene glycol) shell to produce surfactant molecule in situ and to control oil-water interfaces [25].

Elastomeric resins based on VL are commercially available and particularly used as chewing gum base. Specifically, poly(vinyl-acetate)-vinyl laurate (PVAc-VL) has been recently commercialized and is approved for food and drug packaging [12], while it is considered safe in cosmetic formulations [26] and certified with food-contact compliance according to the European Regulation 10/2011 [27]. Currently, PVAc-VL copolymer it is mainly used as a biodegradable chewing gum base to replace polyisoprene-based (synthetic rubber) [28–31]. To the best of our knowledge, it has not been utilized in functional coating formulations. Hence, in this work, we demonstrate this concept by dispersing curcumin in the PVAc-VL copolymer for functionalization.

Curcumin is a natural compound present in a pigment from *Curcuma longa* L (turmeric), widely studied in several fields such as pharmacology [28,29], biomedicine [30], dentistry [31], anti-cancer [32,33], and sensors applications [34]. The use of this molecule was also investigated in food preservation and packaging due to its antioxidant and radical scavenging properties [35], and its antibacterial and bactericidal activity [36,37]. Therefore, curcumin was widely used as additive in composites films for packaging applications. For instance, Zia et al. presented an active food packaging composite film made of low-density polyethylene and curcumin that increased the water vapor barrier properties of the composites [38]. Roy et al. incorporated curcumin in carbohydrate-based composite films to have strong antioxidant and some antimicrobial activity [39], also Roy et al. added curcumin into gelatin composite films [40] or polylactic acid films [41] to improve mechanical, water vapor barrier and UV-barrier properties while maintaining the transparency of the films. Suaza et al. reinforced *Aloe vera*-starch composite films with curcumin-loaded starch nanoparticles and the resultant composite films had lower water vapor permeability [42]. Chen et al. combined curcumin and anthocyanins in starch/polyvinyl alcohol blends to make pH-sensing composite films to monitor the real-time freshness of fish products [43]. Curcumin was used as an additive in coating for food packaging, as well. In addition, Quilez-Molina et al. developed cellulose-polycaprolactone composites with curcumin that can detect pH changes in food [44]. Ghosh et al. developed an edible coating using curcumin doped iron-functionalized cellulose nanofibers and chitosan biocomposites to maintain the quality of kiwifruits during storage [45]; Alohesseini et al. loaded curcumin in gelatin-based and zein-based coatings, revealing promising release behavior in contact with different food simulants [46]; Chen et al. fabricated photoinduced antibacterial PVAc-curcumin coatings for active packaging applications [47].

In this work, we used the food-grade copolymer PVAc-VL and curcumin to develop functional and sustainable coatings, for the first time. We showed the biodegradable solvent 4-methyl-2-pentanone (MIBK, see: Environmental Health Criteria 117 by World Health Organization, 1990; https://apps.who.int/iris/bitstream/handle/10665/39851/9241571179-eng.pdf (last accessed March 2022) is a suitable solvent for both curcumin and the copolymer, and the coatings can be easily applied by dip coating technique. The elastomeric coating was applied not only on solid surfaces like glass, but also on natural substrates, like gelatin and alginate films. Furthermore, these functional coatings demonstrate effective, antioxidant, UV-blocking and low bacterial adhesion properties while improving wettability and barrier properties of natural polymers films. Therefore, this functional coating can be a cost effective alternative in food packaging applications.

2. Materials and methods

2.1. Materials

Poly(vinyl-acetate)-vinyl laurate copolymer (PVAc-VL; VINNAPAS® B 500/40 VL) was purchased from Wacker Chemie AG (viscosity: 8.0–12.0 mPa·s; molecular weight: 320,000 g/mol; glass transition temperature: 0 °C). Curcumin, 4-methyl-2-pentanone (methyl isobutyl ketone, MIBK), ethanol, alginic acid sodium salt, gelatin from cold-water fish skin and glycerol were purchased from Sigma Aldrich. All chemicals are analytical grade and used as received. Deionized water was obtained from Milli-Q Advantage A10 purification system.

2.2. Preparation of the solution

Curcumin (1 g) was dissolved in 4-methyl-2-pentanone (100 mL) after stirring for 2 h at room temperature to obtain 1% (w/v) curcumin solution. Afterward, PVAc-VL (10 g) was added to the curcumin solution until complete polymer dissolution after stirring for 2 h at room temperature. This kind of solution produced a polymer coating containing 10 wt% curcumin upon drying. Concentration details of other formulations including control solutions like pure PVAc-VL solutions are summarized in Table 1. For instance, the samples labeled as PC 10 (polymer-curcumin 90:10) indicated a dry coating with 10 wt% of curcumin, or PC 2.5 indicated a dry coating with 2.5 wt% of curcumin; and finally PC 10A or PC 10G indicate the PC 10 coating applied on alginate (A) or gelatin (G), respectively.

2.3. Preparation of the alginate and gelatin films

Glycerol (0.5 g) was mixed with deionized water (100 mL) at room temperature. Afterward, alginic acid sodium salt (3 g) was dissolved in the previous solution under shaking overnight at room temperature to obtain a 3% (w/v) sodium alginate solution. Likewise, 3% (w/v) gelatin solution was made. 70 mL of the solution were cast on squared Petri-dish (12 cm × 12 cm), previously covered with a layer of PDMS, and dried under an aspirated hood for 24 h. The thicknesses of alginate and gelatin films were measured to be 145 ± 20 μm and 155 ± 35 μm, respectively.

2.4. Preparation of the coatings

Microscope glass slides were dip-coated in 20 mL of various solutions for 30 s and left to dry under an aspirated hood for 24 h in standard conditions (21–23 °C, 40–50% R.H.). The coatings were made with PC 10 (8 ± 2 μm, thick), PC 0 (8 ± 2 μm, thick) and PC 100, respectively. Similarly, alginate films and gelatin films were dip-coated in the same solutions to apply the coatings. Fig. 1 summarizes the solution and coating preparation processes schematically.

Table 1
Coating labels and dry weight percentages. Coatings in the last four rows were made for detailed UV filtering measurements on quartz slides as substrates.

Sample label	Substrate	% PVAc-VL (dry coating)	% curcumin (dry coating)
PC 0	Glass	100	0
PC 100	Glass	0	100
PC 10	Glass	90	10
PC 0A	Alginate	100	0
PC 10A	Alginate	90	10
PC 0G	Gelatin	100	0
PC 10G	Gelatin	90	10
PC 1.25	Quartz	98.75	1.25
PC 2.5	Quartz	97.5	2.5
PC 5	Quartz	95	5
PC 7.5	Quartz	92.5	7.5

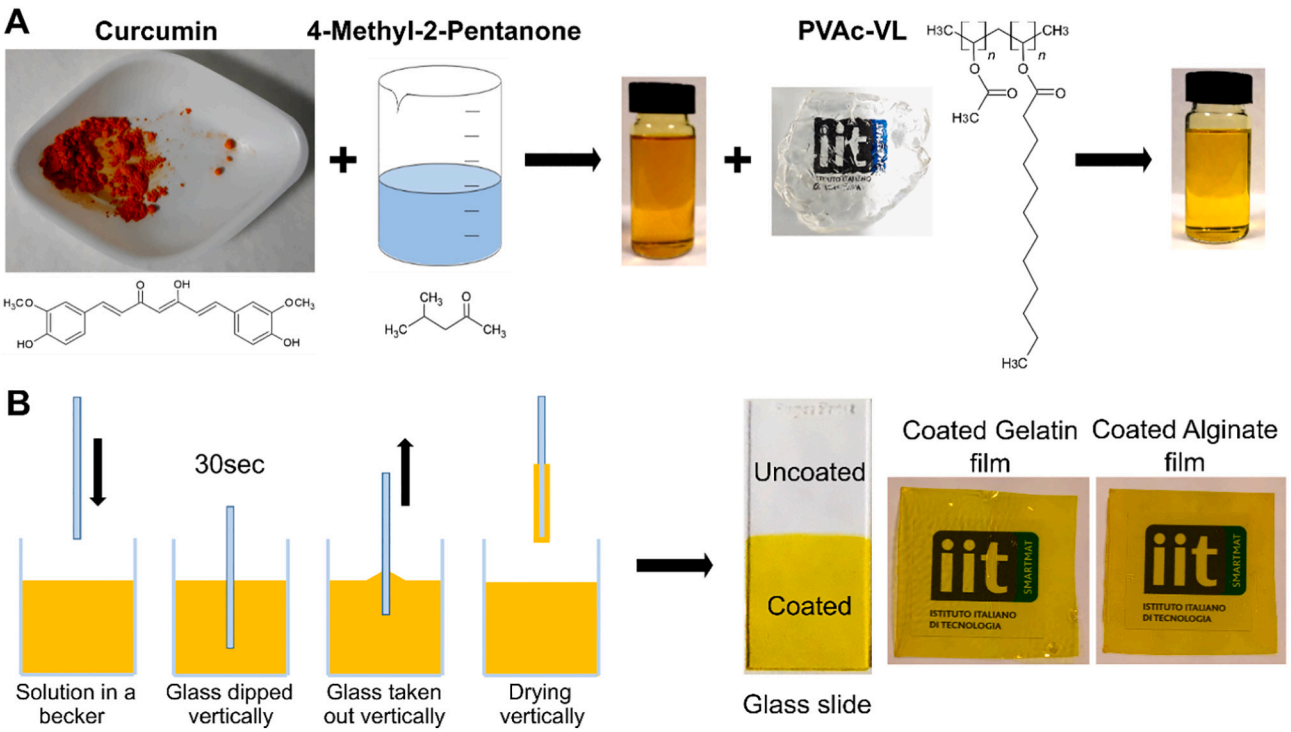

Fig. 1. (A) Schematic illustration of solution fabrication steps. (B) Schematic illustration of the dip coating steps. The photos show coatings on glass (PC 10), gelatin (PC 10G) and alginate (PC 10A).

2.5. Morphological characterization

Scanning electron microscope JSM-6490LA (JEOL, Tokyo, Japan) was used to investigate the microstructure of the surface and cross-section of PC 100, PC 0, PC 10, pure alginate film, PC 10A, pure gelatin film and PC 10G with 5 kV acceleration voltage. The samples were previously mounted on a tilted stub, framed with silver paste, and sputter-coated by using a Cressington Sputter Coater – 208 HR (Cressington, Watford, UK) with a 10 nm thick layer of gold. An AFM system XE-100 (Park Scientific, Suwon, South Korea) with a NCHR probe (f = 320 kHz, c = 42 N/m) was used to investigate the topography of PC 100, PC 0, PC 10. Areas of 5 × 5 μm (256 × 256 pixels) were scanned. The images were acquired in non-contact mode and then processed by Gwyddion software.

2.6. UV–Vis absorbance, light transmittance, and opacity

A Varian CARY 6000i Scan UV–Vis spectrophotometer (Walnut Creek, CA, USA) was used to investigate the absorbance, transparency, and UV-blocking properties of the coatings. The spectral region scanned was from 200 to 800 nm. To study the transparency and the UV-blocking properties of the coatings, the light transmittance was measured. In particular, the transmittance at 660 nm (T_{660}) and 280 nm (T_{280}) of the coatings was evaluated, following the protocol of Roy et al. [39]. Coatings were made on quartz slides. An uncoated quartz slide was used as a reference to perform the measurements.

On the other hand, the opacity was calculated at 600 nm as indicated in previous works [48,49] using the following equation:

$$\text{Opacity} = \frac{\text{Abs}_{600}}{\text{X}} \times 100$$

where Abs_{600} is the value of absorbance at 600 nm and X is the thickness of the coating (mm).

2.7. Yellowness and whiteness index

The yellowness (YI) and whiteness (WI) indexes, of PC 10, pure alginate film, PC 10A, pure gelatin film and PC 10G were evaluated. Photographs of the samples were processed by using a free app "RGB Color Detector" for Android to obtain R, G and B values from all samples. These values were converted from RGB to CIELAB values using a free online color converter (http://colormine.org/convert/rgb-to-lab) and YI and WI values were estimated by using the following equations reported in previous works [41,50], respectively:

$$\text{YI} = \frac{142.86 \times \text{b}}{\text{L}}$$

$$\text{WI} = \text{L} - 3 \times \text{b}$$

where L is the lightness and b is the yellowness/blueness. A sheet of printing paper was used as white support for the samples to take the pictures. Three different samples from each film and three different zones on each sample were photographed to ensure reliable results.

2.8. Chemical characterization

Chemical characterization of curcumin, PVAc-VL (polymer resin), PC 0, PC 10, pure alginate film, PC 10A, pure gelatin film and PC 10G, was performed by using a single-reflection ATR accessory with a diamond crystal (MIRacle ATR, Pike Technologies) coupled to FTIR spectrophotometer (VERTEX 70v FTIR, Bruker). The spectral region scanned was 4000–600 cm^{-1} with a resolution of 4 cm^{-1}. The spectra were normalized to their maximum.

A Horiba Jobin-Yvon μRaman LabRAM HR800 (Horiba Scientific, Kioto, Japan) operating with a He—Ne laser source (632.8 nm) was used to study further the molecular vibration modes of curcumin, PC 0, and PC 10. The objective used was a 50× with a slit aperture of about 150 μm. The spectral region scanned was 3500–1000 cm^{-1} with a resolution of 1 cm^{-1}. The spectra were normalized with maximum absorption peaks.

2.9. Thermal characterization

Thermogravimetric analysis (TGA) of curcumin, PVAc-VL, and PC 10 samples were carried out by using a TGA Q500 (TA Instruments, USA) instrument. Measurements were performed placing the samples (4–7 mg) in platinum pans under inert N_2 flow (50 mL/min) in a temperature range from 30 to 800 °C with a heating rate of 10 °C/min.

2.10. Mechanical characterization

The Young's modulus of PC 0 and PC10 coatings applied on glass slides was measured with an AFM Nanowizard III-JPK (Bruker, Billerica, MA, USA), operated in nano-indentation mode called QI. The system was placed on an active anti-vibration platform inside an anti-acoustic box. A probe CP-NHC-BSG-C-5 (sQUBE, Germany) with a tapping silicon cantilever (thickness 4 ± 1 μm, length 125 ± 10 μm, width 30.0 ± 7.5 μm, resonance frequency 204–497 kHz, spring constant 10–130 N/m) and a borosilicate glass bead of 20 μm diameter as the tip was used for the indentation. The cantilever was calibrated to obtain the actual sensitivity and spring constant. Regions with 5 μm × 5 μm area were scanned with a rate of 0.5 Hz. For each area, 64 force-distance curves (8 × 8 array) were acquired, and three different areas were scanned. The force versus indentation curves were analyzed using the Hertz model with the Poisson's ratio taken as 0.3.

Coatings applied on alginate and gelatin films were tested with uniaxial tension tests on a dual column universal testing machine Instron 3365 (Instron, Norwood, MA, USA) as composites (coating and substrate). Namely, pure alginate film, PC 10A, pure gelatin film and PC10G were cut in dog bone specimens (ten samples tested for statistical analysis) with a width of 4 mm and length of 25 mm. They were conditioned at 24 °C and 50% R.H. in an Espec SH-262 Environmental Chamber (ESPEC, Hudsonville, MI, USA). Displacement was applied at a rate of 3 mm/min. The Young's modulus, stress at maximum load, and elongation at break were calculated from the stress–strain curves.

2.11. Water contact angle

Static water contact angles of PC 0, PC 10, pure alginate film, PC 0A, PC 10A, pure gelatin film, PC 0G, and PC 10G were measured by using a contact angle goniometer OCA-20 (DataPhysics Instruments GmbH, Filderstadt, Germany) at room temperature. Deionized water droplets of 3 μL were deposited on the surface and the contact angle was calculated from the side view with the help of the built in software. Six measurements for each coating were taken to ensure repeatability. In addition, to evaluate eventual water absorption by the coatings, dynamic contact angles of PC 0, PC 100, and PC 10 coatings were measured by dispensing 3 μL volume of deionized water droplets and the contact angles were measured at different time points (0, 1, 2, 3, 4, 5, 10, 15, and 20 min). A sheet of PTFE film was used as a reference. Six measurements were performed for each coating.

2.12. Water vapor permeability measurements

The water vapor permeability (WVP) of pure alginate film, PC 0A, PC 10A, pure gelatin film, PC 0G and PC 10G was evaluated under 100% relative humidity gradient ΔRH (%) by following the ASTM E96 standard method. In detail, 400 μL of deionized water were placed in the permeation chambers (inner diameter = 7 mm; height = 10 mm) to generate 100% R.H. Samples were mounted on the top of the permeation chamber, sealed and placed at 0% R.H. by using anhydrous silica gel. The chambers were weighted every hour for 7 consecutive hours by using a sensitive electronic balance (0.0001 g of accuracy) to monitor the transfer of water from the chamber to the desiccant, through the sample, evaluating the water mass loss, which was plotted as a function of time. The slope of each line was calculated by linear regression. Afterwards, the water vapor transmission rate (WVTR) was determined by using the following equation:

$$\mathrm{WVTR}\left(\mathrm{g}\left(\mathrm{m}^2\ \mathrm{d}\right)^{-1}\right) = \frac{\mathrm{slope}}{\mathrm{A}}$$

where A is the area of the sample.

The water vapor permeability (WVP) of the samples was calculated by using the following equation:

$$\mathrm{WVP}\left(\mathrm{g}\ (\mathrm{m}\ \mathrm{d}\ \mathrm{Pa})^{-1}\right) = \frac{\mathrm{WVTR} \times \mathrm{L} \times 100}{\mathrm{p_s} \times \Delta\mathrm{RH}}$$

where L is the thickness of the sample (m) and p_s is the saturation water vapor pressure at 25 °C (Pa). Each measurement was replicated four times to ensure reliability of the results.

2.13. DPPH and ABTS radical scavenging assays

DPPH (2,2-diphenyl-1-picrylhydrazyl) radical scavenging assay (RSA) was performed with PC 10 samples (2 cm × 2 cm) that were placed in a 6-well plate in a standing position. 12 mL/well of 0.2 mM solution of DPPH• radical molecule in ethanol were added. Samples were covered with aluminum and kept in darkness. 3 mL of extract was taken at specific time points (0, 0.25, 0.5, 1, 2, 3, 4, 6, 24 h), placed in a polystyrene cuvette and its light absorbance was measured at 517 nm by using a Cary 6000i Scan UV–Visible spectrophotometer (Walnut Creek, CA, USA), in dark condition and at room temperature. Separately, PC 0 (2 cm × 2 cm) sample was immersed in 12 mL of DPPH• radical ethanol solution to control if pure PVAc-VL had any antioxidant activity. ABTS (2,2′-azino-bis(e-ethylbenzothiazoline-6-sulphonic acid) radical scavenging assay (RSA) was performed in the same conditions previously described. The percentage RSA was calculated by using the following formula:

$$\mathrm{RSA}\ (\%) = \left[\frac{\mathrm{A_{control}} - \mathrm{A_{sample}}}{\mathrm{A_{control}}}\right] \times 100$$

where $A_{control}$ is the absorption of the control PC 0 sample and A_{sample} is the absorption of the PC 10 sample at the specific time point.

2.14. Release test in food simulants, water and acidic environment

The release of curcumin from PC 10 samples in water, 3% (v/v) acetic acid, 10%, 50% and 95% ethanol-water solutions was measured to simulate aqueous foods (10 vol% ethanol), oil-in-water emulsions (50 vol% ethanol) and fatty foods (95 vol% ethanol), respectively [52,53]. Measurements were made by using a Cary 6000i Scan UV–Visible spectrophotometer (Walnut Creek, CA, USA). Curcumin had a characteristic UV absorbance peak at 428 nm in 3% acetic acid, 10%, 50% and 95% ethanol solutions, whereas presented a peak at 416 nm in water. Calibration curves of curcumin were constructed, to extrapolate the molar extinction coefficient (ε), which resulted in $\varepsilon = 2653\ \mathrm{cm^{-1}\ M^{-1}}$ for 3% acetic acid, $\varepsilon = 2546\ \mathrm{cm^{-1}\ M^{-1}}$ for water, $\varepsilon = 18{,}951\ \mathrm{cm^{-1}\ M^{-1}}$ for 10% ethanol solution, $\varepsilon = 59{,}933\ \mathrm{cm^{-1}\ M^{-1}}$ for 50% ethanol solution and $\varepsilon = 69{,}702\ \mathrm{cm^{-1}\ M^{-1}}$ for 95% ethanol solution. PC 10 samples (2 cm × 2 cm) were placed in a 6-wells plate and immersed in 4 mL of mediums at room temperature. 3 mL of extract was taken at specific time points (0, 0.25, 0.5, 1, 2, 3, 4, 6, 24, and 48 h), and the measurements were carried out. At each time point, 3 mL of respective solution was added to the sample. Six samples for each liquid were analyzed.

2.15. Bacterial adhesion study

The bacterial anti-adhesion property of PC 0, PC 10, and uncoated glass (control) was evaluated by using *Escherichia coli* (*E. coli*) (ATCC 25922) and *Staphylococcus aureus* (*S. aureus*) (8325-4). A single colony of *E. coli* or *S. aureus* was inoculated in Luria-Bertani (LB) broth medium (25 mL) and incubated at 37 °C overnight (o.n.) with shaking at 200

rpm. 1 mL of *E. coli* or *S. aureus* o.n. culture, approximately 10^9 CFU/mL, was centrifuged and suspended in 100 μL of LB. 10 μL of *E. coli or S. aureus* suspension was gently placed, under sterile conditions, onto the PC 0, PC 10, and uncoated glass, previously sterilized by UV irradiation for 30 min. To allow the bacterial adhesion on the material surface, the samples were left to dry for 90 min at room temperature. Afterwards, the bacteria were stained with 0.3% crystal violet (CV) (Merk, Germany) for 15 min to understand if the bacteria adhered to the surface of the samples, following the method previously described with slight modifications [54,55]. To remove unattached or weakly adherent bacteria, the stained samples were carefully rinsed in sterile distilled water (SDW). Then, the uncoated glass, PC 0 and PC 10 were immersed in 25 mL of LB broth and incubated at 37 °C with shaking at 200 rpm. 1 mL of each sample was removed after 1, 2, 3, 4, and 5 h, and the absorbance of the solutions was estimated using a UV–Vis spectrometer at 590 nm (OD_{590}).

To determine the percentage of the adhered bacteria to the samples, the same amount of *E. coli* and *S. aureus* were spotted on PC 0, PC 10, and uncoated glass. The samples were left to dry for 90 min at room temperature. After rinsing with SDW, the adhered bacteria were harvested by detaching with 1 mL of SDW. 10 μl of the *E. coli* or *S. aureus* original suspension was added to 1 mL of SDW and used as control. The absorbance of the bacteria solution was measured at 590 nm (OD_{590}). The percentage of adhered bacteria was calculated respect to the control. The results are presented as mean ± the standard error of the mean (SEM). The significance of the differences in the mean values of groups was evaluated using the analysis of variance (one-way ANOVA). Results with a p-value < 0.05 were considered statistically significant.

2.16. Biocompatibility study

2.16.1. Cell culture

Chinese Hamster Ovarian (CHO) cells (ATCCs, UK) were cultured in Dulbecco's modified Eagle medium (DMEM, Euroclone) 10% fetal bovine serum inactivated, and 1% penicillin streptomycin in a humidified incubator at 37 °C and 5% CO_2. All reagents were products of ThermoFisher. CHO cells were seeded in DMEM at a density of 2×10^4 cells mL^{-1} and let to grow until they were confluent. Cells were then treated with trypsin-EDTA, detached, and centrifuged (1000 rpm, 5 min); the cell pellet was re-suspended in DMEM, and the cell density was precisely determined with an automated cell counter. Further, the cell density was precisely adjusted to 400 cell μL^{-1} to conduct the indirect biocompatibility test.

2.16.2. Cell proliferation assay

Prior to conduct the test, PC 0 and PC 10 were sterilized under UV for 30 min, then rinsed with sterile water, and submerged in DMEM culture medium for 48 h. The proliferation assay was performed with an xCELLigence device (ACEA Biosciences) equipped with E-plate 16. The xCELLigence device allows the real-time monitoring of cell viability based on electrical impedance read out. For each condition (i.e., DMEM conditioned with PC 0, DMEM conditioned with PC 10, and normal DMEM) 4 different wells were used. Each of the 4 wells was filled with 150 μL of DMEM (either conditioned or not). After a background measurement, 50 μL of CHO cell suspension in DMEM was added to each well in order to plate 2×10^3 cells/wells. The proliferation assay was run for 50 h in the incubator. Sampling of the cell proliferation was done every 15 min by reading out the impedance of the electrodes and converting it to a dimensionless parameter, named Cell Index (C.I.), proportional to the electrode area covered by the cells [56]. The C.I. matrix was then processed by IgorPro (Wavemetrics). At the end of the experiment, the cells were inspected by fluorescence microscopy. For fluorescence imaging, CHO cells plated on glass coverslips in the identical conditions were fixed using 4% (w/v) Paraformaldehyde (PFA, SCBiotechnology, USA) in 1× Phosphate Buffer Saline (PBS). The cells were washed once with pre-warmed PBS, pH 7.4, and fixed using 4% PFA for 10 min at room temperature. The fixed cells were first permeabilized with 0.1% Triton X-100 in PBS for 3 to 5 min and then incubated for 10 min in 1% w/v bovine serum albumin (BSA) in PBS to reduce nonspecific background. For selective F-actin staining, the cells were stained with Alexa Fluor-647 phalloidin (life Technologies, USA) diluted in PBS 1× and placed at room temperature for 20 min. The nuclei were stained with Hoechst 33342 (ThermoFisher Scientific). The confocal analysis was finally carried out using a Nikon Inverted Microscope TiE equipped with a Nikon Confocal Laser System (Nikon Optical Co., Ltd., Japan) at an excitation wavelength $\lambda_{ex} = 405$ nm, and $\lambda_{ex} = 647$ nm.

3. Results and discussion

3.1. Morphology of the coatings

SEM surface and cross-section morphology micrographs for PC 100, PC 0 and PC 10 coatings are shown in Fig. 2. The PC 100 coating exclusively composed by curcumin formed a relatively compact coating on glass (Fig. 2A). PC 0 coating (Fig. 2B) also appeared uniform with no visible phase separation between VAc and VL segments. Similarly, PC 10 blend coating surface morphology was smooth and uniform without any phase separation issues as seen in Fig. 2C. Cross-section image of PC 100, however, showed a somewhat porous internal structure that might be attributed to the nature of the coating made by sub-microscopic particles of curcumin (Fig. 2D). Fig. 2E and F show uniform cross section for the coatings PC 0 and PC 10, respectively, with a coating thickness of about 10 μm.

Further coating surface analysis (same coatings shown in Fig. 2) was conducted by AFM (see Supporting Information, Fig. S1). Sub-microscopic particulate nature of the PC 100 coating was confirmed by AFM images that indicated higher surface roughness (~0.6 nm) compared to the polymer-based coating PC 10 that demonstrated about 0.1 nm average surface roughness. Nonetheless, the polymeric coatings were highly smooth with no microscale surface rugosity formation after the coating and drying process.

Microscale morphology of the PC 10 coatings applied on natural alginate (PC 10A) and gelatin (PC 10G) films was also inspected by using SEM as shown in Fig. 3. The figure also shows photographs of both coatings (Fig. 3A and D, respectively) that are yellow in color but with a good degree of optical transparency. Additional pictures and SEM images of pure alginate and gelatin films can be found in the Supporting Information (Fig. S2). In general, the alginate film microstructure featured a rougher surface compared to gelatin upon casting from water solutions confirming earlier reported observations [51]. PC 10A and PC 10G coatings were both homogeneous, smooth, and pore-free, as can be noticed in Fig. 3B and E, respectively. The cross-section micrographs of PC 10A and PC 10G are displayed in Fig. 3C and F, respectively, with an average coating thickness of about 5–8 μm. Coatings were homogenous and adhered well to both biodegradable films.

3.2. UV filtering and optical characteristics

In this section, we investigated the UV filtering ability and the transparency of various coatings containing different curcumin concentrations. The full UV–Vis absorption spectra of the coatings PC 100 and PC 10 are briefly discussed herein and are shown in the Supporting Information as Fig. S3. In particular, the spectra of PC 100 and PC 10 are reported in Fig. S3A and B, respectively. For the PC 100 coating, an intense absorption band of curcumin at 431 nm was ascribed to a combination of $\pi \rightarrow \pi^*$ and $n \rightarrow n^*$ transitions, and a weaker band at 267 nm was due to a $\pi \rightarrow \pi^*$ transitions [57]. On the other hand, due to the presence of the co-polymer in PC 10, the curcumin-related absorption bands shifted to 421 nm and 264 nm.

The photograph in Fig. 4A demonstrates the transparency of PC 10 to the naked eye. This property was confirmed by the percent transmittance (%T) spectra of PC 0, PC 1.25, PC 2.5, PC 5, PC 7.5, and PC 10

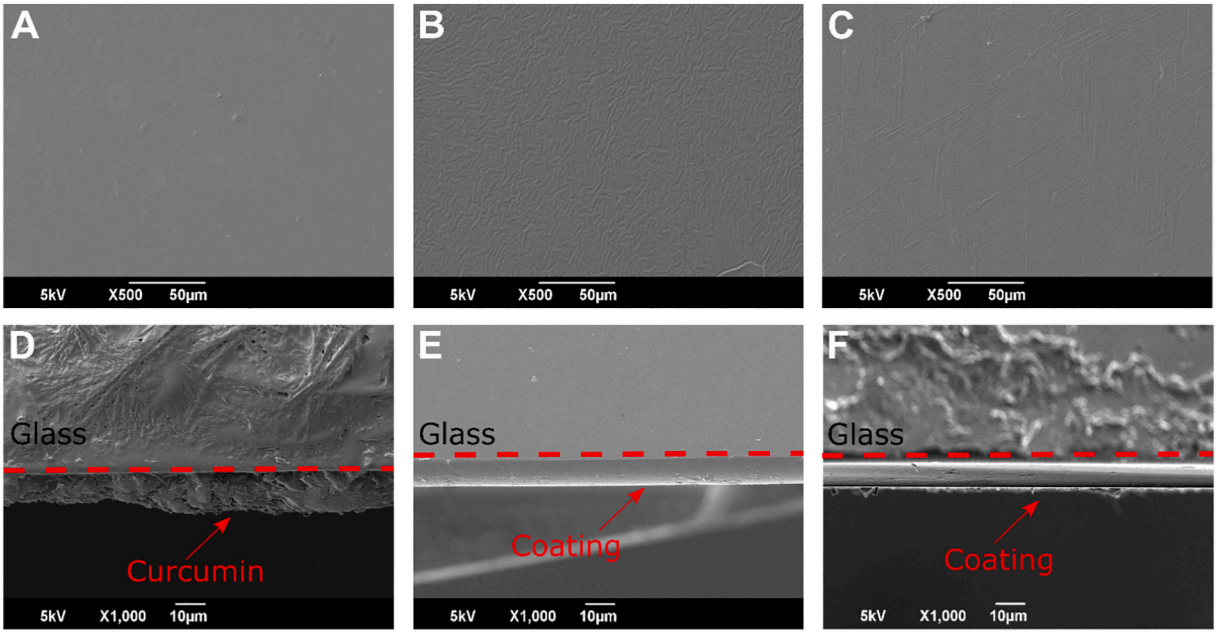

Fig. 2. (A–C) Top view SEM images of PC 100, PC 0 and PC 10. (D–F) Cross section SEM images of PC 100, PC 0 and PC 10.

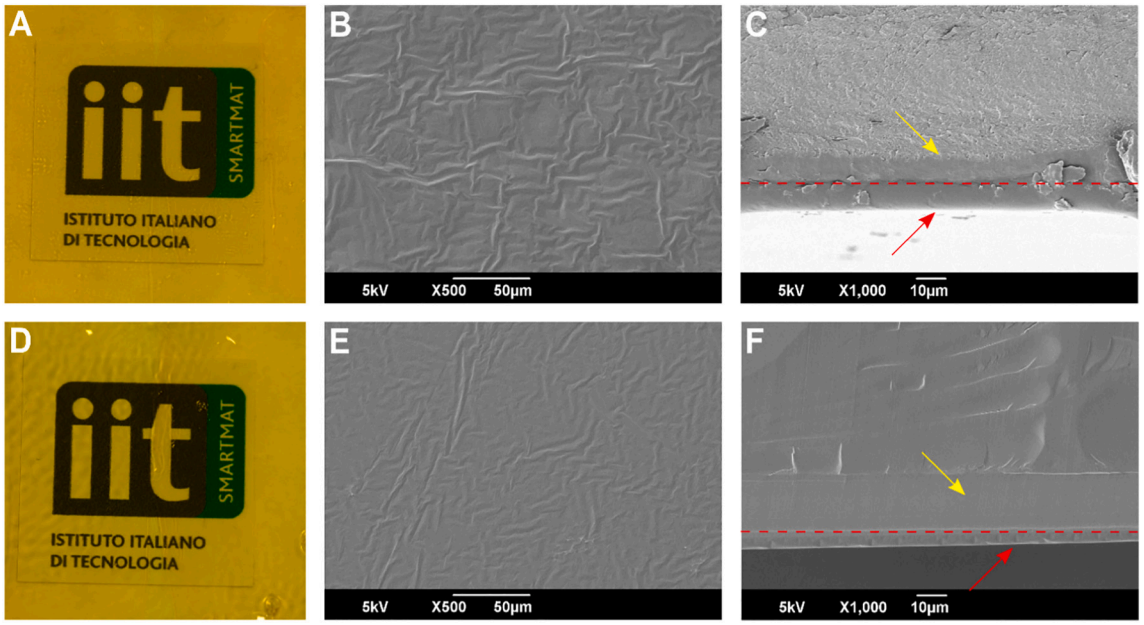

Fig. 3. (A) Photographs of PC 10A. (B) Top view SEM image of PC 10A. (C) Cross section SEM image of PC 10A. (D) Photo of PC 10G. (E) Top view SEM image of PC 10G. (E) Cross section SEM image of PC 10G. The arrows in the figures highlight cutting effects (yellow arrow) and the coating (red arrow and dashed red line) present in the sample. (For interpretation of the references to color in this figure legend, the reader is referred to the web version of this article.)

from 450 to 800 nm shown in Fig. 4B. The spectra indicated that the coatings were transparent in the visible range above 500 nm whereas the pure polymer samples were transparent in all the visible range. We measured the value of $\%T_{660}$ for all the samples that was practically 100% in the visible range. In addition, the percent opacity of the coatings in the visible (600 nm) was also calculated and plotted in Fig. S3C. In particular, PC 0 had the lowest opacity but also all the curcumin-containing coatings' opacity did not exceed 5%.

In Fig. 4C, the %T of all the coatings in the range between 200 nm and 450 nm are shown. Between UVC and UVB bands, the %T increased for all the coatings as the wavelength increased. A minimal increase was observed in PC 10 coating with a maximum of about 30%. At the start of the UVC range, the coatings PC 1.25 and PC 2.5 showed much higher %T values compared to the others indicating insufficient curcumin concentration levels for proper filtering. As a general observation, between UVB and UVA (UVA1) region, the %T decreased for all the coatings except for the pure polymer coating. More specifically, in the UVB region, no significant changes in the %T were measured for all the coatings. The UVA range is classified as UVA2 (320–340 nm) and UVA1 (340–400 nm). In the UVA2 region, the %T of PC 10 ranged from 30 to 16%, while in the UVA1 region, it further declined from 16% and finally to 0% due to high levels of curcumin dispersed in the polymeric matrix [58,59]. The promising effect observed in the UVA region has been as good as other polymer nanocomposites that contain ZnO or TiO_2

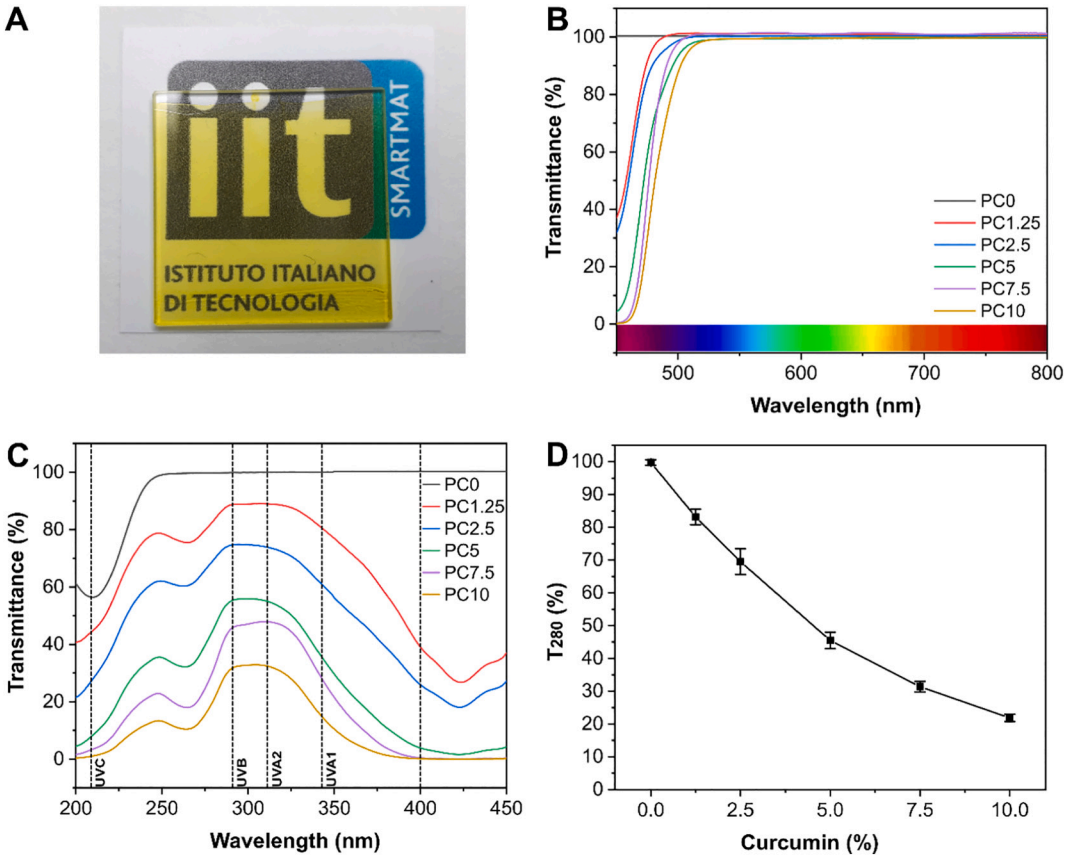

Fig. 4. (A) Photo of PC 10 sample that demonstrates its transparency. (B) Light transmittance (T %) of PC 0, PC 1.25, PC 2.5, PC 5, PC 7.5 and PC 10 in the range 450–800 (Visible range). (C) Light transmittance (T %) of PC 0, PC 1.25, PC 2.5, PC 5, PC 7.5 and PC 10 in the range 200–450 nm (UV range). (D) T_{280} values vs curcumin concentration of PC 0, PC 1.25, PC 2.5, PC 5, PC 7.5 and PC 10.

nanoparticles [60]. The %T at 280 nm was plotted in Fig. 4D to exhibit the UV filtering ability of the coatings as a function of curcumin concentration. As expected, the higher the concentration of curcumin the lower the T_{280} (%), as previously demonstrated by Roy et al. [41]. Therefore, PC 10 demonstrated superior filtering performance compared to all the other coatings produced.

3.3. Yellowness and whiteness index

The surface color values of PC 10, pure alginate film, PC 10A, pure gelatin film and PC 10G are reported in Table 2. As expected, the coated alginate and gelatin films had lower *a* (redness/greenness) and higher *b* (yellowness/blueness) than the uncoated samples, due to the presence of curcumin. In addition, the presence of curcumin significantly increased the YI of PC 10A and PC 10G with respect to the uncoated samples and decreased the WI. As expected, YI indices of PC 10A and PC 10G were higher than the control PC 10, since the natural films have a certain degree of inherent yellowness. Therefore, as can be noticed in Fig. S2A and S2D, pure alginate film appeared brownish whereas gelatin film transparent. The obtained YI of gelatin is comparable to other YI indexes reported for transparent films as well as the effect of curcumin on these indexes [41].

Table 2
Surface color values of PC 10, alginate film, PC 10A, gelatin film and PC 10G. The values are presented as a mean ± standard deviation.

Sample	*L*	*a*	*b*	YI	WI
PC 10	61.60 ± 0.57	−5.28 ± 0.68	46.34 ± 1.67	107.48 ± 4.12	−77.42 ± 5.09
Alginate	56.46 ± 1.62	4.20 ± 0.20	9.02 ± 0.84	22.89 ± 2.76	29.40 ± 4.08
PC 10A	62.86 ± 3.51	−6.12 ± 0.45	61.20 ± 2.62	139.2 ± 2.09	−120.74 ± 4.43
Gelatin	64.32 ± 0.84	5.68 ± 0.23	4.80 ± 0.42	10.66 ± 0.93	49.92 ± 1.47
PC 10G	61.80 ± 1.78	−6.00 ± 0.76	54.86 ± 1.69	126.82 ± 1.82	−102.78 ± 3.58

3.4. Chemical characterization

The coatings under investigation were chemically characterized by ATR-FTIR and Raman spectroscopy. The IR spectra of PVAc polymer (bottom, used as control) and the *co*-polymer PVAc-VL (top) are shown in Fig. S4A (see Supporting Information). The presence of VL was clearly noticed and confirmed in this commercial resin, when compared to pure PVAc. Moreover, the FTIR spectra of PVAc-VL and the coatings PC 0, PC 10, and curcumin are shown in Fig. 5A. The spectrum of curcumin showed the typical bands such as C═C and C═O stretching vibration of the inter-ring chain at 1625 cm^{-1}, C═C stretching vibration of aromatic rings at 1600 cm^{-1}, C═O stretching vibration, C—C—C and C—C═O bending vibration at 1506 cm^{-1}, C—C—C, C—C—H and C—O—H bending vibration of aromatic rings connected with “enolic” part at 1425 cm^{-1}, C—C—C, C—C—H bending vibration of aromatic “keto” part and C—O—H bending vibration of “keto” part at 1278 cm^{-1}, C—O—H bending vibration connected to aromatic rings and of “enolic” form at 1230 cm^{-1}, C—C—H bending vibration at 1203 cm^{-1}, C—O—C bending vibration at 1180 cm^{-1}, C—C—H bending vibration of aromatic rings and C—C—H bending vibration of inter-ring chain at 1149 cm^{-1}, O-CH_3 stretching vibration and C—C—H bending vibration of aromatic ring connected to “enolic” part at 1111 cm^{-1}, C—O—C stretching vibration and C—C—H bending vibration of aromatic ring connected with

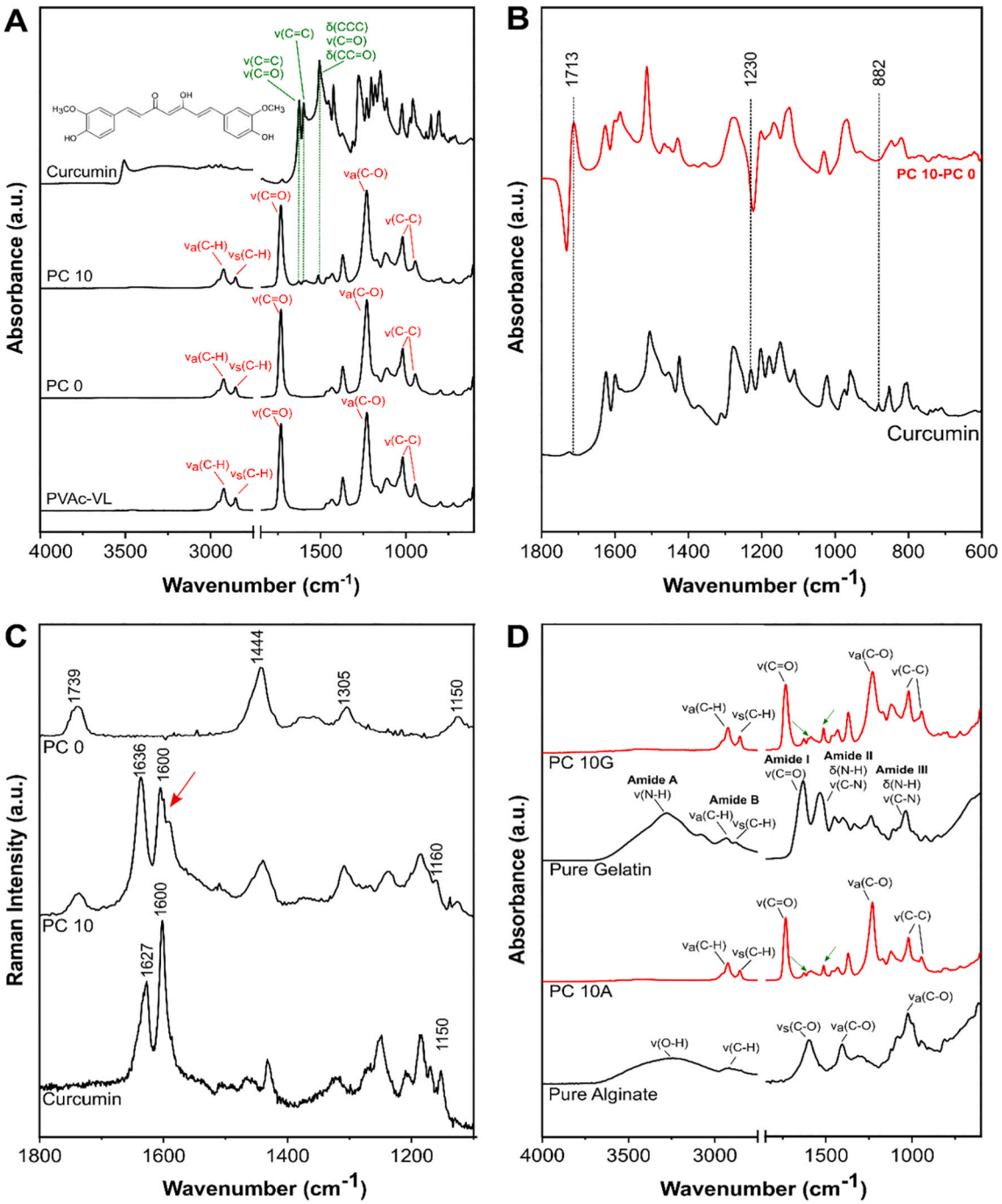

Fig. 5. (A) ATR-FTIR spectra of (from the top) curcumin, PC 10, PC 0 and PVAc-VL. The main assignments of PVAc-VL are reported (red). The assignments of the peaks of PC 10 due to the curcumin are reported (green). (B) ATR-FTIR spectra of curcumin and PC 10–PC 0 in the range 1800–600 cm^{-1}. (C) Raman spectra of (from the bottom) curcumin, PC 10 and PC 0. In PC 10, the red arrow highlights the decrease in the intensity of the peak at 1600 cm^{-1} due to curcumin-polymer interactions. (D) ATR-FTIR spectra of (from the bottom) sodium alginate, PC 10A, gelatin and PC 10G. (For interpretation of the references to color in this figure legend, the reader is referred to the web version of this article.)

"enolic" part at 1022 cm^{-1}, $C^{12}O$ stretching vibration and $C^{12}OH$ bending vibration at 959 cm^{-1}, C—C—H out of plane bending vibration of aromatic ring connected with "enolic" part of the molecule at 881 cm^{-1}, C—C—H out of plane bending vibration of aromatic rings and inter-chain ring at 853 cm^{-1}, C—C—H out of plane bending vibration aromatic ring connected with "keto" part of the molecule at 808 cm^{-1} [61]. Instead, the PC 10 spectrum showed: C—H asymmetric stretching vibration at 2925 cm^{-1}, C—H symmetric stretching vibration at 2854 cm^{-1}, C═O stretching vibration at 1732 cm^{-1}, C═C and C═O stretching vibration at 1628 cm^{-1}, C═C stretching vibration a 1600 cm^{-1}, C═O stretching vibration, C—C—C and C—C═O bending vibration at 1513 cm^{-1}, CH_3 asymmetric and symmetric bending vibration at 1434 and 1370 cm^{-1}, C—O asymmetric stretching vibration at 1229 cm^{-1}, C—O stretching vibration at 1170 and 1119 cm^{-1}, C—C stretching vibration at 1019 and 945 cm^{-1}, and C—H rocking vibration at 797, 721 and 631 cm^{-1}. The peaks at 1628, 1600 and 1513 cm^{-1} were the most evident contribution of the curcumin to PC 10.

In order to understand if there was an interaction between the curcumin and the PVAc-VL co-polymer, the spectrum of PC 0 was subtracted from the spectrum of PC 10. In Fig. 5B this spectrum was

compared with the pure curcumin spectrum. As can be noticed, a peak at 1713 cm^{-1} was visible in the subtracted spectrum but not in the curcumin spectrum. It was assigned to C═O stretching vibration and it is characteristic of the "diketo" form of the curcumin molecule. On the other hand, a peak at 1230 cm^{-1} and a peak at 882 cm^{-1} were visible in the curcumin spectrum but not in the PC 10–PC 0 spectrum. They were assigned to C—O—H bending vibration of the "enolic" part of the molecule and to C—C—H out of-plane bending vibration of the "enolic" part of the molecule, respectively [62]. Therefore, the curcumin molecule changed from the "enolic" form to the "diketo" form (Fig. S4B). This can be attributed to the interactions with the PVAc-VL that are mostly hydrophobic-hydrophobic interactions between the copolymer and the curcumin molecule.

To provide additional information about the molecular interactions between curcumin and PVAc-VL, Raman spectroscopy was used. Fig. 5C shows the Raman spectra of curcumin, PC 10 and PC 0. The spectrum of PC 0 showed: C═O stretching vibration at 1739 cm^{-1}, CH_2 bending vibration at 1444 cm^{-1}, CH_3 bending vibration at 1365 cm^{-1}, C—C stretching vibration at 1305 cm^{-1} and C—O—C stretching vibration at 1126 cm^{-1}. The spectrum of curcumin shows: C═C and C═O stretching vibration of the aromatic ring and ketone group, respectively, at 1627 cm^{-1}, C═C stretching vibration of the aromatic ring at 1600 cm^{-1}, and C—C—H bending vibration of aromatic rings and C—C—H bending vibration of inter-ring chain at 1150 cm^{-1}. In the PC 10 spectra, the peak at 1627 cm^{-1} shifted to 1636 cm^{-1}, and its intensity increased. In addition, the intensity of the peak at 1600 cm^{-1} decreased, and the peak at 1150 cm^{-1} shifted to 1160 cm^{-1}. These changes indicated that there was an interaction between the inter-ring chain and the aromatic rings of the curcumin and PVAc-VL, due to the hydrophobic interactions [61,62].

Fig. 5D shows FTIR spectra of pure alginate, PC 10A, pure gelatin and PC 10G. The spectrum of pure alginate had the typical bands of the sodium alginate: O—H stretching vibration in the range of 3600–3000 cm^{-1}, C—H stretching vibrations at 2927 cm^{-1}, carboxylate salt ion symmetric and asymmetric stretching vibrations at 1598 and 1406 cm^{-1}, respectively, C—O asymmetric stretching vibration at 1023 cm^{-1} [63,64]. The spectrum of pure gelatin displayed [65]: amide A band at 3280 cm^{-1} due to N—H stretching vibration, amide B band at 2933 cm^{-1} due to the C—H stretching vibration, amide I at 1631 cm^{-1} due to C═O stretching vibration, amide II at 1533 cm^{-1} due to NH bend coupled with CN stretch and amide III at 1239 cm^{-1} due to NH bend stretch with CN stretch. The FTIR spectra of the coatings PC 10A and PC 10G did not show any peaks of alginate and gelatin, respectively but had previously described and discussed PVAc-VL and curcumin characteristic peaks. These results suggested that the coatings were homogenous and external coatings that did not mix or dissolved in the pure natural polymers but rather remained as protective layers over the films or the substrates.

3.5. Mechanical characterization

To measure local values of the surface Young's Moduli of PC 0 and PC 10, an AFM indentation technique was used. Table 3 reports measurement details and the calculated errors. The Poisson's ratio was assumed to be 0.3 for both coatings. The sensitivities of PC 0 and PC 10 were comparable. Since these are local measurements, one needs to take as many indentation measurements as possible to obtain statistical figures for both coatings. In Fig. 6A the Young's Modulus for each measurement point of PC 0 (top) and PC 10 (bottom) are reported. Three different and randomly chosen areas of PC 0 and PC 10 were scanned (in black, red and blue), measuring the Young's Modulus of 64 points for each area in an 8 × 8 array. In each area, a mean Young's Modulus is reported (also in the graph). The average of these Young's Moduli was calculated and reported in Table 3 as a single value. The coating surface Young's Moduli of PC 0 and PC 10 were comparable (~3.1 and 4.2 MPa, respectively) and the curcumin did not introduce extra hardness or surface stiffness to the polymer coatings. Calculated percent error was higher in PC 10 due to the dispersion of curcumin in the polymer; however, such error values are considered acceptable for such coating systems [66].

Table 3
Assumed Poisson's ratio, measured sensitivity, measured Young's modulus and calculated percentage measurement error of PC 0 and PC 10 coatings on glass. The Young's modulus is presented as a mean ± standard deviation.

Sample	Poisson's ratio [ν]	Sensitivity (nm/V)	Young's modulus (MPa)	Error (%)
PC 0	0.3	22.4	4.28 ± 0.93	7
PC 10	0.3	23.8	3.14 ± 0.31	25

The mechanical properties of pure alginate film, PC 10A, pure gelatin film and PC 10G were also investigated. Fig. 6B shows the stress-strain curves of the samples. The values of Young's Moduli (YM), the elongation at break and the tensile stress at maximum load of the samples are reported in Table 4. In particular, the YM of pure gelatin was 353.6 ± 65.0 MPa, while PC 10G had YM of 173.9 ± 40.4 MPa. In addition, the elongation at break of gelatin and PC 10G were 96.7 ± 19.2% and 157.7 ± 18.7%, respectively. The tensile stress at maximum load of gelatin and PC 10G were 10.0 ± 1.6 MPa and 10.0 ± 2.8 MPa, respectively. These results suggested that the coating was conformal, well adhered and elasticized pure gelatin film, while keeping the tensile stress at maximum load unchanged. On the other hand, pure alginate had YM of 1282.8 ± 149.0 MPa, while PC 10A had YM of 1229.3 ± 93.5 MPa. The percentage elongation at break of pure alginate and PC 10A were measured to be 9.2 ± 1.5% and 10.8 ± 1.3%, respectively. The tensile stress at maximum load for pure alginate and PC 10A were 36.2 ± 4.2 MPa and 34.7 ± 2.7 MPa, respectively. These results suggested that in the case of alginate the coating did not significantly affect the mechanical properties of the films.

3.6. Thermal stability

The thermal stability of the curcumin powder, PVAc-VL and PC 10 was evaluated by TGA, and the thermograms including the derivative of weight loss curve are reported in Fig. 6C and D, respectively. As can be noticed, curcumin (blue line) started its thermal degradation at ≈190 °C and showed two main degradation events centered at ≈300 °C and ≈400 °C, showing a residual weight of 30% at 800 °C. PVAc-VL (red line) presented two thermal events. Specifically, its degradation started slowly at ≈220 °C. At ≈370 °C its weight loss was approximately 75%. Afterwards, the degradation occurred at different rate until 490 °C, and the final weight loss was 97%. PC 10 weight loss was similar to PVAc-VL: it started its degradation at ≈220 °C, its weight loss was 75% at ≈370 °C and reached 94% after 490 °C. These results suggested that the encapsulated curcumin did not change the thermal stability of the co-polymer, as previously observed [41], therefore it was protected by the polymeric matrix against thermal degradation. These results are better visible in Fig. 6D, where the degradation derivatives shifted by about 70 °C once curcumin was encapsulated within the polymer.

3.7. Static and dynamic wetting properties

The static water contact angles of PC 0, PC 10, pure alginate film, PC 0A, PC 10A, pure gelatin film, PC 0G and PC 10G were measured and reported in Table 5. The hydrophilic behavior of pure alginate film was in accordance to previous results [67], as well as the static contact angle of pure gelatin (close to 80°) could be explained with the orientation of functional groups of hydrophobic amino acids of gelatin into the matrix, as previously reported [68]. As can be noticed, the coating significantly improved the wettability properties of natural films. In addition, the presence of curcumin did not influence the wettability properties of the coatings, whatever was the substrate.

Dynamic contact angles were also evaluated to assess potential

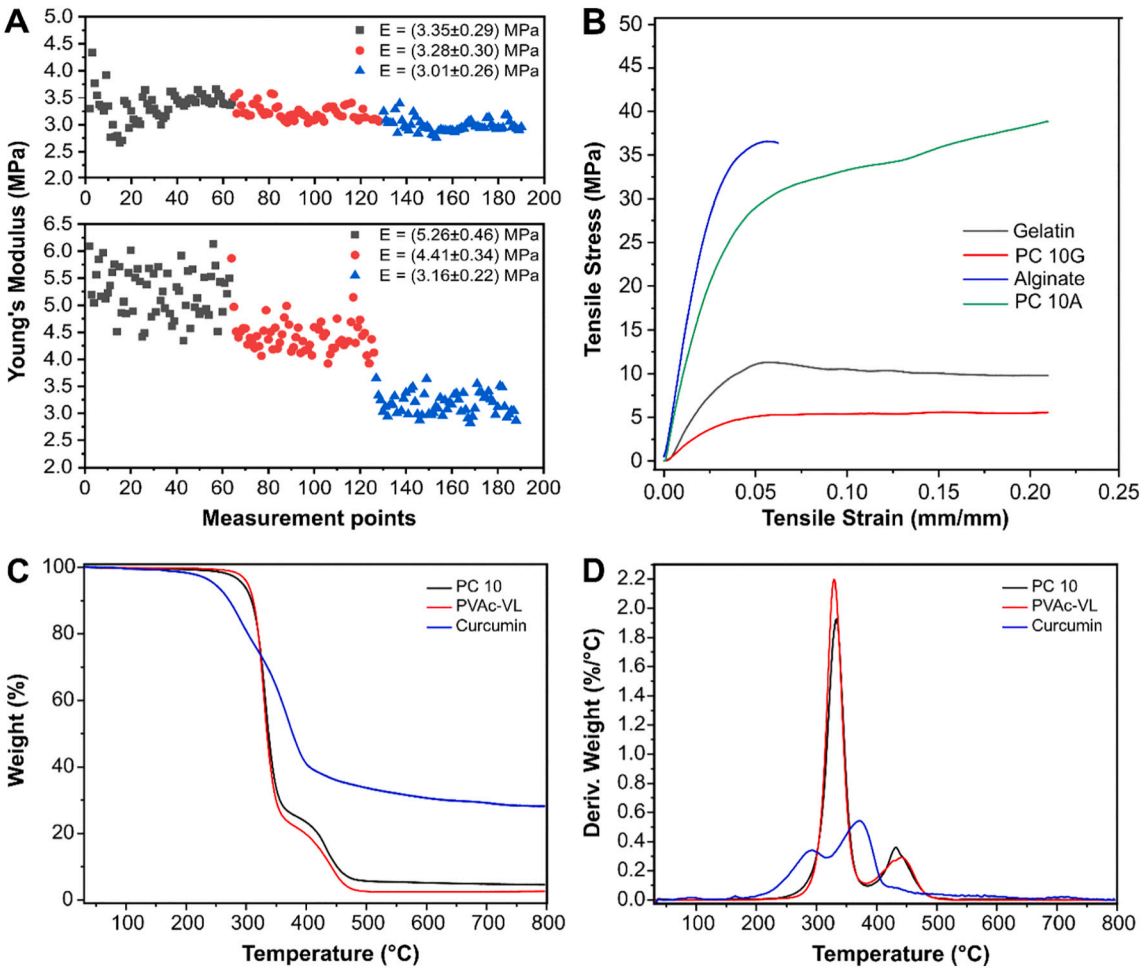

Fig. 6. (A) Young's modulus per each measurement points per each scanned area (black, red and blue) of PC 0 (top) and PC 10 (bottom). (B) Stress-strain curves of pure gelatin film, PC 10G, pure alginate film, PC 10A. (C) Mass loss and (D) derivatives of the thermograms of curcumin (blue), PVAc-VL (red) and PC 10 (black). (For interpretation of the references to color in this figure legend, the reader is referred to the web version of this article.)

Table 4
Young's modulus (MPa), elongation at break (%) and tensile stress at maximum load (MPa) of pure gelatin film, PC 10G, pure alginate film and PC 10A. The values are presented as a mean ± standard deviation.

Sample label	Young's modulus (MPa)	Elongation at break (%)	Tensile stress at maximum load (MPa)
Gelatin	353.6 ± 65.0	96.7 ± 19.2	10.0 ± 1.6
PC 10G	173.9 ± 40.4	157.7 ± 18.7	10.0 ± 2.8
Alginate	1282.8 ± 149.0	9.2 ± 1.5	36.2 ± 4.2
PC 10A	1229.3 ± 93.5	10.8 ± 1.3	34.7 ± 2.7

Table 5
Static contact angle of PC 0, PC 10, pure alginate, PC 0A, PC 10A, pure gelatin, PC 0G, PC 10G. WVTR, WVP of pure alginate, PC 0A, PC 10A, pure gelatin, PC 0G and PC 10G. The values are presented as a mean ± standard deviation.

Sample	CA (°)	WVTR ($g/m^2 \cdot day$)	WVP ($g/m \cdot day \cdot Pa$)
PC 0	86.9 ± 2.0	–	–
PC 10	89.9 ± 1.6	–	–
Pure alginate	54.2 ± 1.8	$(5.92 \pm 0.57) \cdot 10^{3}$	$(2.44 \pm 0.12) \cdot 10^{-4}$
PC 0A	93.9 ± 2.3	$(2.55 \pm 0.48) \cdot 10^{3}$	$(1.86 \pm 0.22) \cdot 10^{-4}$
PC 10A	94.7 ± 3.6	$(2.10 \pm 0.38) \cdot 10^{3}$	$(1.54 \pm 0.36) \cdot 10^{-4}$
Pure gelatin	77.6 ± 5.0	$(5.03 \pm 1.30) \cdot 10^{3}$	$(3.10 \pm 0.37) \cdot 10^{-4}$
PC 0G	98.0 ± 2.0	$(2.17 \pm 0.48) \cdot 10^{3}$	$(1.50 \pm 0.31) \cdot 10^{-4}$
PC 10G	97.5 ± 2.0	$(1.91 \pm 0.19) \cdot 10^{3}$	$(1.33 \pm 0.18) \cdot 10^{-4}$

absorption over time. Fig. 7A shows the dynamic contact angles of PC 100, PC 0, PC 10, as well as PVAc and Teflon as control. As can be seen, in the first 5 min the contact angles of PVAc, PC 0, PC 10 and PC 100 decreased by about ≈8–10° while the Teflon control surface decreased by about 7°. As such, this decline was attributed to water evaporation. On the other hand, from 5 min to 20 min, the contact angle of PC 0 and PC 10 declined by about 50°, the contact angle of PC 100 declined by about 20°, the contact angle of PVAc declined by 30°, and over Teflon the decline was about 20° that is purely evaporation driven. Only, PC 100 dynamic contact angle was comparable to Teflon, while the dynamic contact angles of PC 0 and PC 10 declined much more indicating water absorption by the copolymer. Hence, this copolymer can be classified as hydrophobic but hygroscopic.

3.8. *Barrier properties: water vapor permeability*

The water vapor transmission rate (WVTR) and the water vapor permeability (WVP) of pure alginate, PC 0A, PC 10A, pure gelatin, PC 0G and PC 10G are reported in Table 5. As can be noticed, the WVTR and the WVP decreased in presence of the coatings, but curcumin did not influence the barrier properties of the composites as a confirmation of the good encapsulation without phase separation of the filler curcumin in the polymeric matrix.

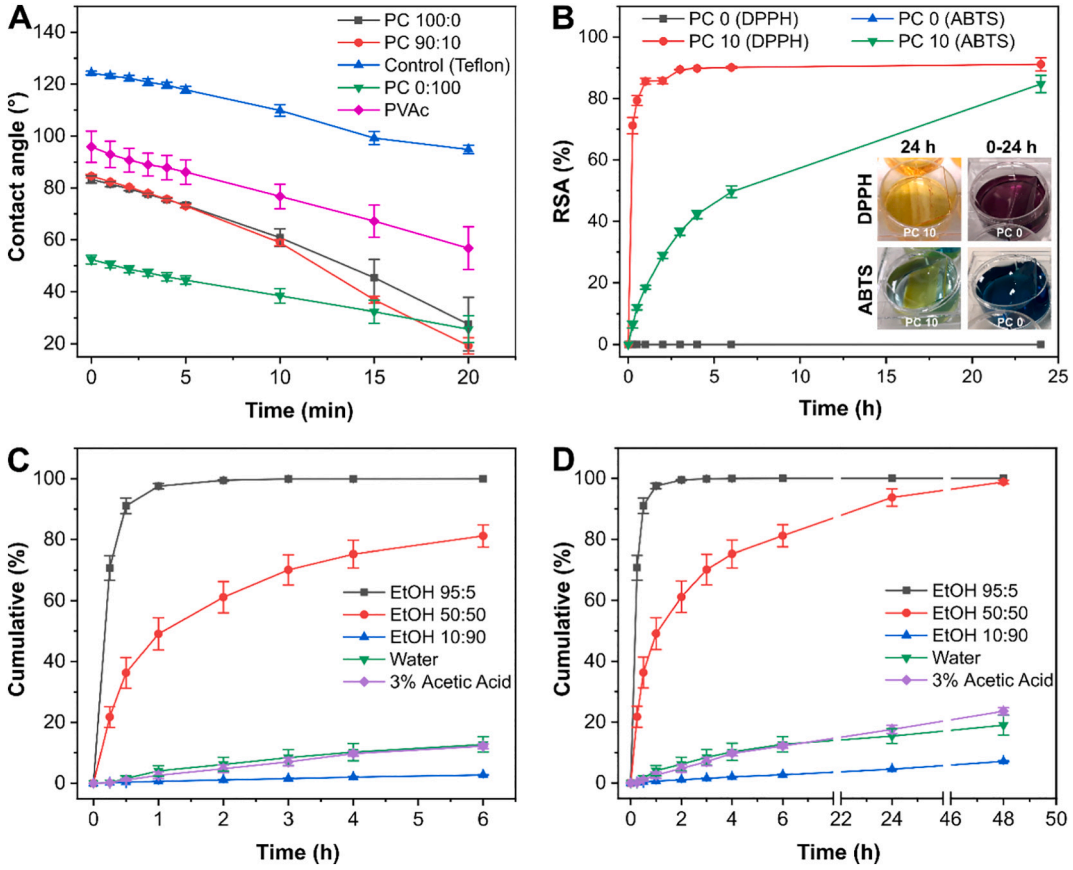

Fig. 7. (A) Dynamic contact angle of (from the top) Teflon (control), PVAc, PC 0, PC 10, PC 100. (B) Radical scavenging activity with DPPH assay of PC 0 (grey) and PC 10 (red). Radical scavenging activity with ABTS assay of PC 0 (blue) and PC 10 (green). In the insert, photos of PC 10 (on the left) and PC 0 (on the right) immersed in the DPPH (up) and ABTS (down) solution safer 24 h are shown at 24 h. (C) Percentage cumulative release of curcumin from PC 10 at 0, 0.25, 0.5, 1, 2, 3, 4 and 6 h in different solutions: EtOH 95:5 (grey), EtOH 50:50 (red), EtOH 10:90 (blue), water (green) and 3% (v/v) acetic acid (purple). (D) Percentage cumulative release of curcumin from PC 10 at 0, 0.25, 0.5, 1, 2, 3, 4, 6, 24 and 48 h in different solutions: EtOH 95:5 (grey), EtOH 50:50 (red), EtOH 10:90 (blue), water (green) and 3% acetic acid (purple). (For interpretation of the references to color in this figure legend, the reader is referred to the web version of this article.)

3.9. Antioxidant activity and release in food simulants

The DPPH and ABTS scavenging activities of PC 10 and PC 0 are reported in Fig. 7B. In the DPPH assay PC 10 demonstrated an RSA of 71 ± 3% and 91 ± 2% after 15 min and 24 h, respectively, whereas in the ABTS assay PC 10 demonstrated an RSA of 7 ± 1% and 85 ± 3% after 15 min and 24 h, respectively. On the other hand, in both assays PC 0 did not show any radical scavenging activity, as can be observed from the graph. These results confirmed the antioxidant activity of the encapsulated curcumin in PC 10 coating.

Percentage cumulative curcumin release data from PC 10 are plotted in Fig. 7C and D. In Fig. 7C, the release in the first 6 h is shown, whereas in Fig. 7D the release was extended to 48 h. In 95% ethanol solution (fatty food simulant), 70% of the curcumin was released in the first 15 min, 90% in 30 min and practically 100% after 1 h. On the other hand, in 50% ethanol solution (emulsion food simulant), 20% of the curcumin was released in the first 15 min, after the first hour only 50% was released, while after 48 h, the 100% of curcumin was released. In 10% ethanol solution (aqueous food simulant), only about 10% of the curcumin was released within 48 h. In acidic condition (3% acetic acid) there was a slight release of curcumin after 30 min (1%) until 23% after 48 h. A similar behavior was observed in water, with a release of 19% after 48 h. The differences in the release rate was previously explained with the diffusion of the active compound in the polymer matrix and with its solubility in the release medium [41]. The high release rate of the curcumin in 95% ethanol was due to its high solubility in the alcoholic solvent. On the contrary, curcumin has very low solubility in water based mediums. No rapid burst release was observed in 50% ethanol solution compared to the 95% strength solution. In addition, different rates and behaviors were observable from the release in 10% ethanol, water and 3% acetic acid solution. All these results indicated that this system allows a controlled release in different conditions, from the emulsified food to acidic environments. Due to hydrophobicity of curcumin it has much slower and perhaps much longer release dynamics in water and weak aqueous acidic solutions compared to water soluble and edible antioxidant pigments [69].

3.10. Bacterial adhesion study

Fig. 8A and B display the growth curves of *S. aureus* and *E. coli*, respectively, on the uncoated glass, used as control, PC 0, and PC 10. The bacterial growth increased exponentially after 2.5 h on uncoated glass. On the other hand, no significant *E. coli* and *S. aureus* growth was observed for PC 0 and PC 10 after 5 h. These results indicated anti-adhesion properties of the coatings, as can be confirmed by the photos, which show a higher adhesion of the bacteria on glass than on PC 0, and PC 10. Indeed, the purple spot due to the crystal violet staining was clearly visible on glass, differently from treated samples, for both bacteria strains. The brownish color of the spot on PC 10 was due to the change in color of curcumin because of the basic environment created by the crystal violet. Therefore, the spot did not represent adhered bacteria, but simply the curcumin color change in response to the pH of the staining medium.

In addition, the percentage of bacterial adhesion was evaluated

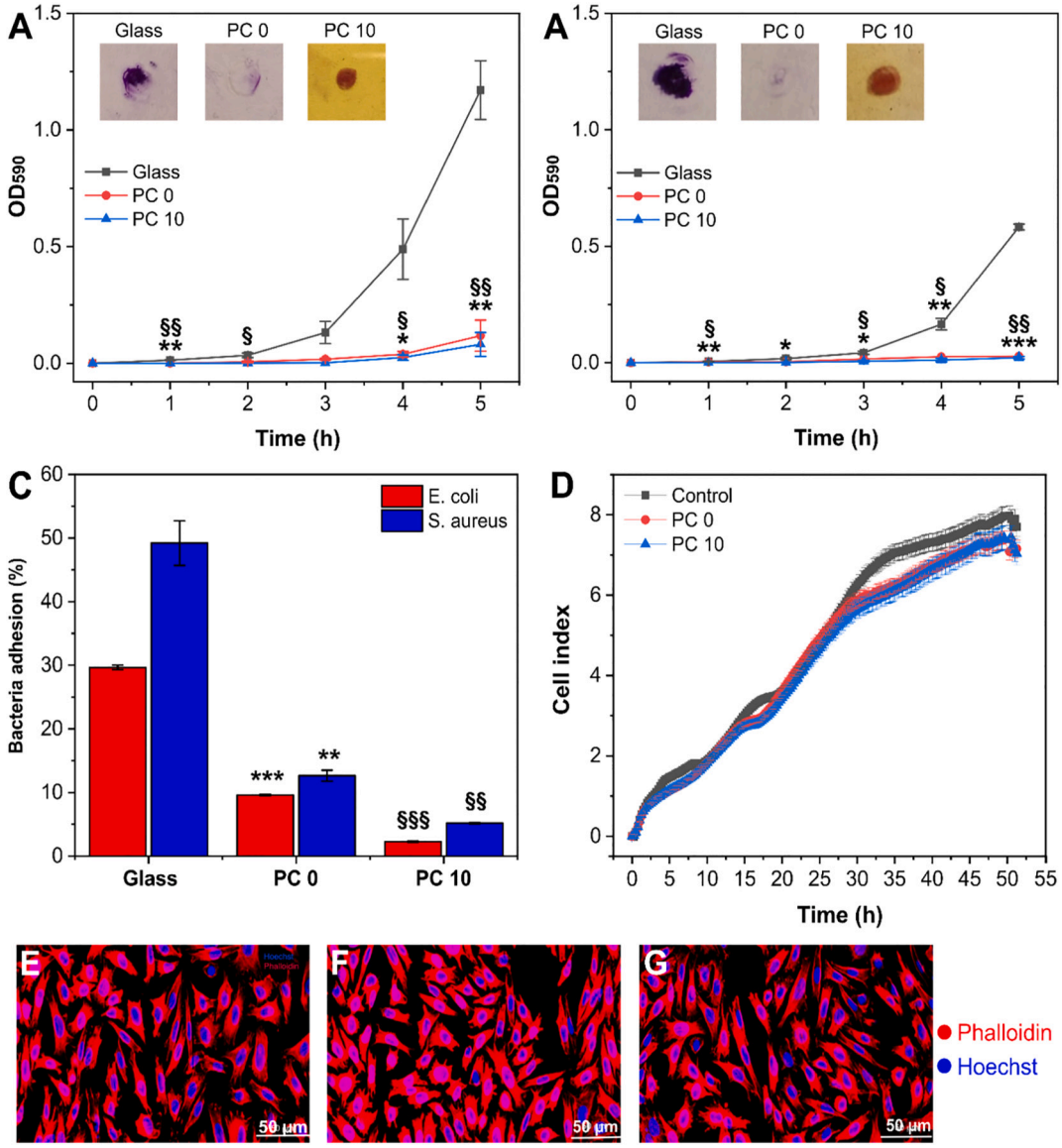

Fig. 8. (A) Bacterial growth (*S. aureus*) on uncoated glass (black), PC 0 (red) and PC 10 (blue), and photos of the samples after staining with CV of the adhered bacteria and rinsing with SDW. (B) Bacterial growth (*E. coli*) on uncoated glass (black), PC 0 (red) and PC 10 (blue), and photos of the samples after staining with CV of the adhered bacteria and rinsing with SDW. (C) Percentage bacteria adhesion on glass, PC 0 and PC 10 for *S. aureus* (red) and *E. coli* (blue). The values are presented as a mean ± standard error of the mean of at least 3 independent experiments. *($p < 0.05$), **($p < 0.01$), ***($p < 0.001$): PC 0 vs glass. § ($p < 0.05$), §§ ($p < 0.01$), §§§ ($p < 0.001$): PC 10 vs glass. (D) The real-time proliferation curves measured for CHO growing in normal culture medium (DMEM, control) in black, in DMEM conditioned with PC 0 in red, and in DMEM conditioned with PC 10 in blue. (E) Confocal images of CHO cells growing in normal DMEM (control). (F) Confocal images of CHO cells growing in DMEM conditioned with PC 0. (G) Confocal images of CHO cells growing in DMEM conditioned with PC 10. Cells nuclei are labeled with Hoechst (blue), and the cytoskeleton is labeled with Phalloidin (red). (For interpretation of the references to color in this figure legend, the reader is referred to the web version of this article.)

(Fig. 8C). In particular, *S. aureus* adhered stronger (45.7%) than *E. coli* (30%) to the glass surface, suggesting that higher adhesiveness of this strain was probably due to the different polysaccharides structural components of its cell wall [54]. However, a considerable reduction in adhesion to the PC 100 and PC 10 surface respect to the glass was observed for both the bacteria strains. Moreover, the adhesion on PC 10 was lower than PC 0 due to the presence of curcumin, which was demonstrated to have antibacterial properties [70–72].

3.11. Biocompatibility study

The indirect biocompatibility test was performed via a proliferation assay conducted in culture medium previously conditioned with PC 0 and PC 10 samples. In this way it was possible to determine if toxic chemical reagents were released by the materials, affecting cell viability. The results (i.e., the recorded C.I. vs. t) are reported in Fig. 8D. The graph shows that the proliferation phase started shortly after the adhesion of the cells to the electrodes and rapidly increased until the cells were confluent onto the electrodes after 50 h. No differences were detected between control (i.e., CHO cultured in normal DMEM) and CHO cells cultured in conditioned DMEM. In particular, the curves obtained in PC 0 and PC 10 conditioned media are perfectly superimposable. As it is evident also from the fluorescence images acquired at the end of the proliferation tests (Fig. 8E–G) cell survival and proliferation were allowed in the culture medium conditioned in the materials. The fluorescence images showed no differences in the cell shape and morphology.

4. Conclusions

A functional coating was developed using an elastomeric copolymer, PVAc-VL and curcumin that can be applied on various surfaces such as solid glass and natural alginate and gelatin films, by using dip-coating technique. Curcumin was effectively dispersed in the coatings and as a result coating transparency was maintained while filtering out significant portions of UV light. This effect can prevent light-induced degradation of the underlying substrates or of the packaged food. Coatings demonstrated strong antioxidant activity and curcumin was released from the coatings in various media in a sustained manner. The coatings appeared to improve the mechanical, hydrophobic and barrier properties of the substrates. The coatings were not toxic to cell proliferation and they prevented the adhesion of *E. coli* and *S. aureus* bacterial colonies. These outcomes suggest that these coatings can be used in food preservation and packaging applications.

CRediT authorship contribution statement

Marta Fadda: Investigation, Methodology, Writing – original draft. **Marco Contardi:** Investigation, Writing – review & editing. **Silvia Dante:** Investigation, Writing – original draft, Writing – review & editing. **Marta Di Carlo:** Investigation, Writing – original draft, Writing – review & editing. **Giacoma Galizzi:** Investigation. **Athanassia Athanassiou:** Investigation, Writing – review & editing. **Ilker S. Bayer:** Conceptualization, Methodology, Writing – review & editing, Supervision.

Declaration of competing interest

The authors declare that they have no known competing financial interests or personal relationships that could have appeared to influence the work reported in this paper.

Acknowledgment

The authors would like to thank Dr. Lara Marini (Smart Materials, IIT) for thermo-gravimetric analysis measurements, Dr. Riccardo Carzino (Smart Materials, IIT) for the Raman Spectroscopy measurement, Dr. Luca Caruana (IRIB, CNR) for technical support in bacterial adhesion study, and Mechanical Characterization Facility (IIT), especially Dr Marco Salerno for AFM measurements.

Appendix A. Supplementary data

Supplementary data to this article can be found online at https://doi.org/10.1016/j.porgcoat.2022.106883.

References

[1] N. Lavrov, Vinyl acetate copolymer-based adhesive materials, Polym Sci Ser C 49 (3) (2007) 255–257.
[2] N. Zhang, et al., Application of polyvinyl Acetate/Lignin copolymer as bio-based coating material and its effects on paper properties, Coatings 11 (2) (2021) 192.
[3] C.M. Liauw, et al., The effect of surface hydrophobicity on the attachment of fungal conidia to substrates of polyvinyl acetate and polyvinyl alcohol, J. Polym. Environ. 28 (5) (2020) 1450–1464.
[4] N. Zhang, et al., The copolymer of polyvinyl acetate containing lignin-vinyl acetate monomer: synthesis and characterization, Eur. Polym. J. 123 (2020), 109411.
[5] A. Kaboorani, et al., Nanocrystalline cellulose (NCC): a renewable nano-material for polyvinyl acetate (PVA) adhesive, Eur. Polym. J. 48 (11) (2012) 1829–1837.
[6] N. Friis, A. Hamielec, Kinetics of vinyl chloride and vinyl acetate emulsion polymerization, J. Appl. Polym. Sci. 19 (1) (1975) 97–113.
[7] N. Grassie, I. McLean, I. McNeill, Thermal degradation of vinyl chloride-vinyl acetate copolymers—I. Bulk degradation studies by thermal volatilization analysis, Eur. Polym. J. 6 (5) (1970) 679–686.
[8] A. Brar, S. Charan, Sequence determination of vinyl acetate–methyl acrylate copolymers by NMR spectroscopy, J. Appl. Polym. Sci. 53 (13) (1994) 1813–1822.
[9] S. Duquesne, et al., Vinyl acetate/butyl acrylate copolymers—part 1: mechanism of degradation, Polym. Degrad. Stab. 83 (1) (2004) 19–28.
[10] W. Stark, M. Jaunich, Investigation of ethylene/vinyl acetate copolymer (EVA) by thermal analysis DSC and DMA, Polym. Test. 30 (2) (2011) 236–242.
[11] C. Schneider, et al., Applications of ethylene vinyl acetate copolymers (EVA) in drug delivery systems, J. Control. Release 262 (2017) 284–295.
[12] O. Chaabouni, S. Boufi, Cellulose nanofibrils/polyvinyl acetate nanocomposite adhesives with improved mechanical properties, Carbohydr. Polym. 156 (2017) 64–70.
[13] S. Samaha, H. Nasr, A. Hebeish, Synthesis and characterization of starch-poly (vinyl acetate) graft copolymers and their saponified form, J. Polym. Res. 12 (5) (2005) 343–353.
[14] L. Chen, et al., Synthesis and characterization of starch-g-poly (vinyl acetate-co-butyl acrylate) bio-based adhesive for wood application, Int. J. Biol. Macromol. 114 (2018) 1186–1193.
[15] T.-M. Don, C.-F. King, W.-Y. Chiu, Preparation of chitosan-graft-poly (vinyl acetate) copolymers and their adsorption of copper ion, Polym. J. 34 (6) (2002) 418–425.
[16] M. Silva, et al., Characterization of poly (vinyl acetate)/sugar cane bagasse lignin blends and their photochemical degradation, J. Therm. Anal. Calorim. 106 (2) (2011) 407–413.
[17] W. Mormann, M. Al-Higari, Acylation of starch with vinyl acetate in water, Starch-Stärke 56 (3–4) (2004) 118–121.
[18] L. Junistia, et al., Synthesis of higher fatty acid starch esters using vinyl laurate and stearate as reactants, Starch-Stärke 60 (12) (2008) 667–675.
[19] B.A. Lina, H. Messinger, A. Bär, 13-week oral toxicity study of vinyl laurate in rats, Regul. Toxicol. Pharmacol. 71 (1) (2015) 101–107.
[20] H. Messinger, A. Bär, Subchronic toxicity, toxicity to reproduction and prenatal developmental toxicity of vinyl laurate, Regul. Toxicol. Pharmacol. 70 (1) (2014) 80–86.
[21] P. Kraisomdet, et al., Amphiphilic dextran-vinyl laurate-based nanoparticles: formation, characterization, encapsulation, and cytotoxicity on human intestinal cell line, Progr. Biomater. (2020) 1–9.
[22] S. Sun, et al., A thermoresponsive chitosan– NIPAAm/vinyl laurate copolymer vector for gene transfection, Bioconjug. Chem. 16 (4) (2005) 972–980.
[23] N. Abidi, E. Hequet, Cotton fabric graft copolymerization using microwave plasma. II. Physical properties, J. Appl. Polym. Sci. 98 (2) (2005) 896–902.
[24] L. Benee, M. Snowden, B. Chowdhry, Novel gelling behavior of poly (N-isopropylacrylamide-co-vinyl laurate) microgel dispersions, Langmuir 18 (16) (2002) 6025–6030.
[25] B.S. Aldakkan, et al., Stimuli-responsive, hydrolyzable poly (Vinyl laurate-co-vinyl Acetate) nanoparticle platform for in situ release of surfactants, ACS Appl. Mater. Interfaces 13 (21) (2021) 25553–25562.
[26] Amended final safety assessment of polyvinyl acetate, Journal of the American College of Toxicology 15 (2) (1996) 166–176.
[27] Commission Regulation (EU) No 10/2011, 2011, 14 January.
[28] D.-C. Kim, S.-K. Ku, J.-S. Bae, Anticoagulant activities of curcumin and its derivative, BMB Rep. 45 (4) (2012) 221–226.
[29] S. Kulkarni, A. Dhir, K.K. Akula, Potentials of curcumin as an antidepressant, Sci. World J. 9 (2009) 1233–1241.
[30] R.S. Virk, et al., Curcumin-containing orthopedic implant coatings deposited on poly-ether-ether-ketone/bioactive glass/hexagonal boron nitride layers by electrophoretic deposition, Coatings 9 (9) (2019) 572.
[31] D. Murgia, et al., Development of a multifunctional bioerodible nanocomposite containing metronidazole and curcumin to apply on L-PRF clot to promote tissue regeneration in dentistry, Biomedicines 8 (10) (2020) 425.
[32] B.B. Aggarwal, A. Kumar, A.C. Bharti, Anticancer potential of curcumin: preclinical and clinical studies, Anticancer Res. 23 (1/A) (2003) 363–398.
[33] R. Wilken, et al., Curcumin: a review of anti-cancer properties and therapeutic activity in head and neck squamous cell carcinoma, Mol. Cancer 10 (1) (2011) 1–19.
[34] M.Y. Khorasani, et al., The role of curcumin and its derivatives in sensory applications, Mater. Sci. Eng. C 103 (2019), 109792.
[35] T. Ak, İ. Gülçin, Antioxidant and radical scavenging properties of curcumin, Chem. Biol. Interact. 174 (1) (2008) 27–37.
[36] S.-Y. Teow, et al., Antibacterial action of curcumin against Staphylococcus aureus: a brief review, J. Trop. Med. 2016 (2016).
[37] P. Tyagi, et al., Bactericidal activity of curcumin I is associated with damaging of bacterial membrane, PloS one 10 (3) (2015), e0121313.
[38] J. Zia, et al., Low-density polyethylene/curcumin melt extruded composites with enhanced water vapor barrier and antioxidant properties for active food packaging, Polymer 175 (2019) 137–145.
[39] S. Roy, J.-W. Rhim, Preparation of carbohydrate-based functional composite films incorporated with curcumin, Food Hydrocoll. 98 (2020), 105302.
[40] S. Roy, J.-W. Rhim, Preparation of antimicrobial and antioxidant gelatin/curcumin composite films for active food packaging application, Colloids Surf. B: Biointerfaces 188 (2020), 110761.
[41] S. Roy, J.-W. Rhim, Preparation of bioactive functional poly (lactic acid)/curcumin composite film for food packaging application, Int. J. Biol. Macromol. 162 (2020) 1780–1789.
[42] L. Nieto-Suaza, et al., Characterization of Aloe vera-banana starch composite films reinforced with curcumin-loaded starch nanoparticles, Food Struct. 22 (2019), 100131.
[43] H.-Z. Chen, et al., Novel pH-sensitive films containing curcumin and anthocyanins to monitor fish freshness, Food Hydrocoll. 100 (2020), 105438.
[44] A.I. Quilez-Molina, et al., Responsive bio-composites from magnesium carbonate filled polycaprolactone and curcumin-functionalized cellulose fibers, Adv. Sustain Syst. 5 (10) (2021) 2100128.

[45] T. Ghosh, K. Nakano, V. Katiyar, Curcumin doped functionalized cellulose nanofibers based edible chitosan coating on kiwifruits, Int. J. Biol. Macromol. 184 (2021) 936–945.
[46] A. Alehosseini, et al., Electrospun curcumin-loaded protein nanofiber mats as active/bioactive coatings for food packaging applications, Food Hydrocoll. 87 (2019) 758–771.
[47] L. Chen, et al., Photoinduced antimicrobial activity of curcumin-containing coatings: molecular interaction, stability and potential application in food decontamination, ACS Omega 5 (48) (2020) 31044–31054.
[48] J.A. Heredia-Guerrero, et al., All-natural sustainable packaging materials inspired by plant cuticles, Adv. Sustain. Syst. 1 (1–2) (2017) 1600024.
[49] S.A. Oleyaei, et al., Synergistic reinforcing effect of TiO2 and montmorillonite on potato starch nanocomposite films: thermal, mechanical and barrier properties, Carbohydr. Polym. 152 (2016) 253–262.
[50] R. Hirschler, Whiteness, yellowness, and browning in food colorimetry: a critical review, Color Food (2012) 118–129.
[51] Astm, Standard test method for oxygen gas transmission rate through plastic film and sheeting using a coulometric sensor, in: Annual Book of American Standard Testing Methods, 1995, pp. 472–477.
[52] M.H. Lee, S.Y. Kim, H.J. Park, Effect of halloysite nanoclay on the physical, mechanical, and antioxidant properties of chitosan films incorporated with clove essential oil, Food Hydrocoll. 84 (2018) 58–67.
[53] P. Ezati, J.-W. Rhim, pH-responsive chitosan-based film incorporated with alizarin for intelligent packaging applications, Food Hydrocoll. 102 (2020), 105629.
[54] G.B. Hwang, et al., The anti-biofouling properties of superhydrophobic surfaces are short-lived, ACS Nano 12 (6) (2018) 6050–6058.
[55] S. Naderizadeh, et al., Bioresin-based superhydrophobic coatings with reduced bacterial adhesion, J. Colloid Interface Sci. 574 (2020) 20–32.
[56] N. Ke, et al., The xCELLigence system for real-time and label-free monitoring of cell viability, in: Mammalian Cell Viability, Springer, 2011, pp. 33–43.
[57] E. López-Tobar, et al., Encapsulation and isomerization of curcumin with cyclodextrins characterized by electronic and vibrational spectroscopy, Vib. Spectrosc. 62 (2012) 292–298.
[58] X. Liu, et al., Protective effect of curcumin against ultraviolet a irradiation-induced photoaging in human dermal fibroblasts, Mol. Med. Rep. 17 (5) (2018) 7227–7237.
[59] H. Li, et al., Protective effect of curcumin against acute ultraviolet B irradiation-induced photo-damage, Photochem. Photobiol. 92 (6) (2016) 808–815.
[60] A.I. Quilez-Molina, et al., UV-blocking, transparent, and antioxidant polycyanoacrylate films, Polymers 12 (9) (2020) 2011.
[61] K. Hu, et al., Core–shell biopolymer nanoparticle delivery systems: synthesis and characterization of curcumin fortified zein–pectin nanoparticles, Food Chem. 182 (2015) 275–281.
[62] T.M. Kolev, et al., DFT and experimental studies of the structure and vibrational spectra of curcumin, Int. J. Quantum Chem. 102 (6) (2005) 1069–1079.
[63] H. Daemi, M. Barikani, Synthesis and characterization of calcium alginate nanoparticles, sodium homopolymannuronate salt and its calcium nanoparticles, Sci. Iran. 19 (6) (2012) 2023–2028.
[64] A. Jejurikar, et al., Degradable alginate hydrogels crosslinked by the macromolecular crosslinker alginate dialdehyde, J. Mater. Chem. 22 (19) (2012) 9751–9758.
[65] L. Cai, et al., Characterization of gelatin/chitosan ploymer films integrated with docosahexaenoic acids fabricated by different methods, Sci. Rep. 9 (1) (2019) 1–11.
[66] M. Salerno, Improved estimation of contact compliance via atomic force microscopy using a calibrated cantilever as a reference sample, Measurement 45 (8) (2012) 2103–2113.
[67] G. Tedeschi, et al., Sustainable fabrication of plant cuticle-like packaging films from tomato pomace agro-waste, beeswax, and alginate, ACS Sustain. Chem. Eng. 6 (11) (2018) 14955–14966.
[68] P.V. Pulla-Huillca, et al., Wettability of gelatin-based films: the effects of hydrophilic or hydrophobic plasticizers and nanoparticle loads, J. Food Eng. 297 (2021), 110480.
[69] G. Bayer, A. Shayganpour, J. Zia, I.S. Bayer, Polyvinyl alcohol-based films plasticized with an edible sweetened gel enriched with antioxidant carminic acid, J. Food Eng. 1 (323) (2022 Jun), 111000.
[70] S.-H. Mun, et al., Synergistic antibacterial effect of curcumin against methicillin-resistant Staphylococcus aureus, Phytomedicine 20 (8–9) (2013) 714–718.
[71] D.G. Yun, D.G. Lee, Antibacterial activity of curcumin via apoptosis-like response in Escherichia coli, Appl. Microbiol. Biotechnol. 100 (12) (2016) 5505–5514.
[72] H. Wang, et al., Release kinetics and antibacterial activity of curcumin loaded zein fibers, Food Hydrocoll. 63 (2017) 437–446.